Irreducible gravitational wave background as a particle detector

Anish Ghoshal,[1,*] Angus Spalding,[2,†] and Graham White[2,‡]

[1]*Department of Physics and Astronomy, University of Sussex, Brighton, BN1 9RH, United Kingdom*
[2]*School of Physics and Astronomy, University of Southampton, Southampton SO17 1BJ, United Kingdom*

(Received 6 June 2026; accepted 28 August 2026; published 22 September 2026)

Beyond the standard model particles can imprint a temporary early matter-dominated epoch on a stochastic gravitational-wave background. For a freely propagating background whose production has ceased, we show that the resulting feature contains two characteristic frequencies that determine the particle decay rate Γ and the abundance-weighted mass $Y_i M$, independently of the microphysical origin of the gravitational-wave source. Using numerical scans, we derive semianalytic relations between these characteristic frequencies and the beyond the standard model particle parameters, and quantify the parameter ranges over which these relations remain valid. For backgrounds that remain actively sourced, the end of early matter domination continues to define a source-independent cosmological frequency scale controlled by Γ, although the second feature, and hence the inference of $Y_i M$, is source dependent. Once a particle model and production mechanism are specified, the measured combinations can be translated into masses and microscopic couplings. Remarkably, decay lengths targeted by upcoming long-lived-particle searches map directly onto the nanohertz range in which NANOGrav has reported evidence for a stochastic gravitational-wave background.

DOI: 10.1103/3d8p-8q4v

I. INTRODUCTION

Stochastic gravitational-wave (GW) backgrounds provide us a unique opportunity to probe the early Universe, as they carry crucial information from pre–big bang nucleosynthesis epochs that are otherwise inaccessible [1–5]. Consequently, the study of gravitational-wave backgrounds has become a major focus of current research, with next generation experiments expected to probe 12 decades of frequencies with sufficient GW strain sensitivity to shed light on the conditions of the first second of the Universe [6–31]. The LIGO–Virgo Collaboration [6,7] detected gravitational waves from black hole mergers a decade ago, while pulsar timing array collaborations have very recently reported strong evidence for a stochastic GW background at the nano-Hertz frequency [24–28,32,33].

These results have stimulated a wide range of beyond–Standard Model possibilities for cosmological GW production in the early Universe. The majority of these sources are transient, meaning they are no longer being sourced in our context, in particular primordial tensor modes from inflation [1,34–38], first-order phase transitions [34,39], and annihilating domain walls [40–43]. This is unlike for instance domain walls before annihilation [44] and cosmic string gravitational wave sources [45].

In the standard cosmological history after reheating, the Universe is radiation dominated until relatively late times, implying that gravitational-wave energy densities redshift with the same rate as the dominant background, so it remains constant in time. However, any deviation from standard radiation domination modifies this behavior [46–54]. A temporary change in the equation of state alters the relative redshifting between gravitational waves and the background energy density, imprinting a characteristic distortion on the observed GW spectrum [37,55–63].

In this regard, we consider a period of early matter domination induced by heavy metastable particles [64–77]. Such long-lived particles (LLPs) are well motivated in many extensions of the Standard Model, including models of neutrinos [65,78,79], axions [80], supersymmetry [54], extra dimensions [81], and dark matter [65,80], and are the focus of a rapidly expanding experimental program [82–87]. Dedicated searches, including MATHUSLA, DUNE, and SHiP, are expected to significantly extend the sensitivity of these searches in the coming years [88–94]. Massive particle species with sufficiently small decay rates naturally redshift slower than radiation and can temporarily dominate the energy density of the Universe before decaying back into the thermal bath sourcing a period of early matter domination.

*Contact author: A.Ghoshal@sussex.ac.uk
†Contact author: angus.spalding1@gmail.com
‡Contact author: G.A.White@soton.ac.uk

Published by the American Physical Society under the terms of the Creative Commons Attribution 4.0 International license. Further distribution of this work must maintain attribution to the author(s) and the published article's title, journal citation, and DOI. Funded by SCOAP³.

TABLE I. Comparison with closely related studies of early matter domination and gravitational-wave backgrounds. Previous works have considered specific BSM particles generating early matter domination and specific gravitational wave background (GWB) sources; the present work generalizes these scenarios and provides an updated analysis.

Work	GWB source	BSM particle
Ref. [79]	Inflation	Right-handed neutrinos
Ref. [65]	Cosmic strings	Right-handed neutrinos
Present work	Generic GWB	Generic BSM particle

Such a deviation from standard radiation domination imprints two characteristic features in the GW background spectrum, corresponding to the onset and termination of the nonstandard period [79,80,95–103]. We show that these features in the GW spectrum encode the mass, decay width, and initial abundance of the long-lived particles. In particular, the two characteristic frequencies map directly to the decay rate Γ and the product MY_i. Consequently, within a given particle physics model, measuring these frequencies enables the underlying Lagrangian parameters, such as the particle mass and couplings governing the decay rate, to be inferred.[1] A schematic illustration of this inference chain from gravitational wave observables to particle physics parameters is shown in Fig. 5. Production mechanisms include, but are not limited to, thermal production with freeze-out [65], inflaton decay [64,109], number changing scattering processes [110], the misalignment mechanism [111–114], and gravitational production during inflation [115,116].

The imprint of early matter domination on gravitational-wave backgrounds from long-lived particles has previously been studied in specific right-handed-neutrino scenarios for inflationary backgrounds [81] and cosmic-string backgrounds [65]. Here, we generalize this framework to arbitrary gravitational-wave backgrounds and to any beyond the standard model (BSM) particle capable of generating an early matter-dominated epoch, while providing an updated and improved numerical analysis. This is shown in Table I.

This paper is organised as follows. In Sec. II, we study early matter domination driven by BSM particles, derive the conditions under which it occurs, and track the evolution of the equation-of-state parameter numerically. In Sec. III, we show that the resulting gravitational-wave feature is characterized by two frequencies and obtain numerical semi-analytic relations connecting them to the underlying model parameters. Finally, we conclude in Sec. IV.

[1]We should note that the decay of long-lived particles can themselves generate a gravitational wave background either via graviton Bremmstrahlung [78,104–106] or via decay to gravitons [107,108]; however these are in the frequency range several orders larger than those considered in this work.

II. EARLY MATTER DOMINATION FROM BSM PARTICLES

In this section we analyze how a long-lived particle species can generate a temporary period of early matter domination. We first derive analytic expressions describing the scaling behavior of the system, obtaining relations for the temperature at which the species begins to dominate the energy density, $T_{\rm dom}$, and the temperature at which its decay restores radiation domination, $T_{\rm end}$, in terms of the particle mass, initial abundance, and decay rate. We then numerically solve the Boltzmann equations governing the evolution of the matter and radiation energy densities.

A. Analytic approximations

We consider a general BSM particle species X of mass M that is decoupled from the thermal bath while still relativistic and subsequently evolves independently of the radiation plasma. The comoving number density of X is characterized by its initial yield $Y_i \equiv n_X/s$, where s is the entropy density. When the species behaves as matter the corresponding energy densities of matter and radiation are

$$\rho_X = Mn_X = MY_i s, \qquad \rho_R = \frac{\pi^2}{30} g_* T^4, \tag{1}$$

with $s = (2\pi^2/45) g_* T^3$ assuming no entropy dumps occur. The ratio then evolves as

$$\frac{\rho_X}{\rho_R} = \frac{MY_i s}{\rho_R} = \frac{4}{3} Y_i \frac{M}{T}, \tag{2}$$

which grows as the temperature decreases. Matter domination occurs when $\rho_X = \rho_R$, defining

$$T_{\rm dom} \simeq \frac{4}{3} Y_i M. \tag{3}$$

Having found the temperature at which the particle dominates the energy budget of the Universe we now look to find when it stops dominating the Universe returning to radiation domination. This calculation is much simpler as we simply match the decay rate to the Hubble parameter at the decay temperature

$$\Gamma = H(T_{\rm end}) = \sqrt{\frac{4\pi^3 g_*}{45}} \frac{T_{\rm end}^2}{M_{\rm Pl}}. \tag{4}$$

Rearranging for $T_{\rm end}$ gives

$$T_{\rm end} = \left(\frac{45}{4\pi^3 g_*}\right)^{1/4} \sqrt{\Gamma M_{\rm Pl}} \simeq 0.24 \sqrt{\Gamma M_{\rm Pl}}. \tag{5}$$

Having found the analytic approximations we now find the relations numerically.

B. Numerical results

The above analysis is useful to understand the scaling of the parameters and give analytical estimates; however to determine accurately when matter domination begins and ends to determine the evolution of the equation of state we numerically solve the Boltzmann system for the energy densities for the thermal bath ρ_R and the species X ρ_X:

$$\dot{\rho}_X + 3H(w_X + 1)\rho_X = -\Gamma_X(\rho_X - \rho_X^{eq}) \tag{6}$$

$$\dot{\rho}_R + 4H\rho_R = \Gamma_X(\rho_X - \rho_X^{eq}). \tag{7}$$

The Hubble parameter, H, is given by the Friedmann equation

$$H(t) = \sqrt{\frac{8\pi}{3M_{\rm Pl}^2}(\rho_X + \rho_R)}. \tag{8}$$

The equilibrium radiation energy density is determined by the temperature

$$\rho_R(T) = \frac{\pi^2}{30} g_* T^4. \tag{9}$$

The average energy per particle is calculated following Maxwell-Bolztmann statistics and is dependent on the mass of the particle and the temperature

$$\langle E_X \rangle = M_X \frac{K_1(M_X/T)}{K_2(M_X/T)} + 3T, \tag{10}$$

which allows us to calculate the equation of state parameter w_X,

$$w_X = \frac{P_X}{\rho_X} = \frac{n_X T}{n_X \langle E_X \rangle} = \frac{T}{\langle E_X \rangle}. \tag{11}$$

This value interpolates between radiation $w = 1/3$ at $T \gg M$ and matter $w = 0$ at $T \ll M$. Then the total equation of state parameter of the Universe is given by

$$w_{\rm tot} = \frac{w_X \rho_X + (1/3)\rho_R}{\rho_X + \rho_R}. \tag{12}$$

The equilibrium energy density similarly calculated in terms of the particle mass and the temperature,

$$\rho_X^{\rm eq}(T) = \frac{g_X}{2\pi^2} M_X^2 T K_2\left(\frac{M_X}{T}\right)\left[M_X \frac{K_1(M_X/T)}{K_2(M_X/T)} + 3T\right]. \tag{13}$$

We provide a typical benchmark of the evolution of these variables in Fig. 1.

Initially $T \gg M_X$ so the energy density redshifts with radiation. Then once $T \lesssim M$ X behaves like matter and the energy density redshifts slower than radiation and comes to dominate the Universe. The Hubble parameter first shifts as radiation, then after $T_{\rm dom}$ shifts as matter domination, and finally as Hubble drops below Γ_X then the decays of X occur significantly. The abundance and physical energy densities then drop to a negligible amount, and the Hubble redshifts like radiation again. The temperature drops until decays begin which can be seen as the point where Y_X starts decreasing, and then radiation injection occurs slowing the decrease of the temperature. Then once the decays are complete the temperature shifts with expansion. The equation of state parameter begins with radiation domination at $w = 1/3$; then as the particle acts like matter and comes to dominate the energy budget of the Universe the equation of state parameter drops to zero, and then when decays begin and the Universe becomes radiation dominated the equation of state rises up to $w = 1/3$ again. The red dotted line shows our analytical estimates. The analytic estimate agrees well with the numerical result throughout the matter-dominated era, but becomes inaccurate during the transition back to radiation domination because it assumes that the decay of X occurs instantaneously. In what follows we shall use the numerical results at all time rather than the analytic estimates.

To find best fits to the domination and decay temperatures we scan over the parameters Y, M, Γ and plot $T_{\rm dom}$ against (M, Y) and $T_{\rm end}$ against Γ to show the dependencies derived are correct and find best fits to the prefactors. The best-fit relations extracted from the numerical scan shown in Fig. 2 are

$$T_{\rm dom} = \frac{4}{3} Y_i M, \qquad T_{\rm end} = 0.15\sqrt{\Gamma M_{\rm Pl}}. \tag{14}$$

The corresponding logarithmic coefficients of determination coincide, $R^2_{\log} = 0.999996$, demonstrating excellent agreement between the numerical results and the expected analytic scaling. The discrepancies between the numerical results and the analytic estimates arise from the simplifying assumptions used in the analytic derivations. In estimating the end of the matter-dominated era, we assume that the decay occurs instantaneously when $\Gamma_X = H$. In reality the decay proceeds continuously over a finite interval, so radiation domination is restored only after further evolution. To ensure that X decays only after it has come to dominate the energy density, we require $T_{\rm end} < T_{\rm dom}$. This gives

$$\frac{\Gamma M_{\rm Pl}}{Y_i^2 M^2} < \left(\frac{4}{3 \times 0.15}\right)^2 \simeq 79. \tag{15}$$

This expression makes explicit the dependence on both the initial abundance Y_i and the particle mass M, and therefore applies to both thermal and nonthermal production scenarios. To illustrate the resulting constraint, we consider two examples:

(1) For thermally produced right-handed neutrinos,

$$\Gamma_N = \frac{\tilde{m} M^2}{8\pi v^2}, \tag{16}$$

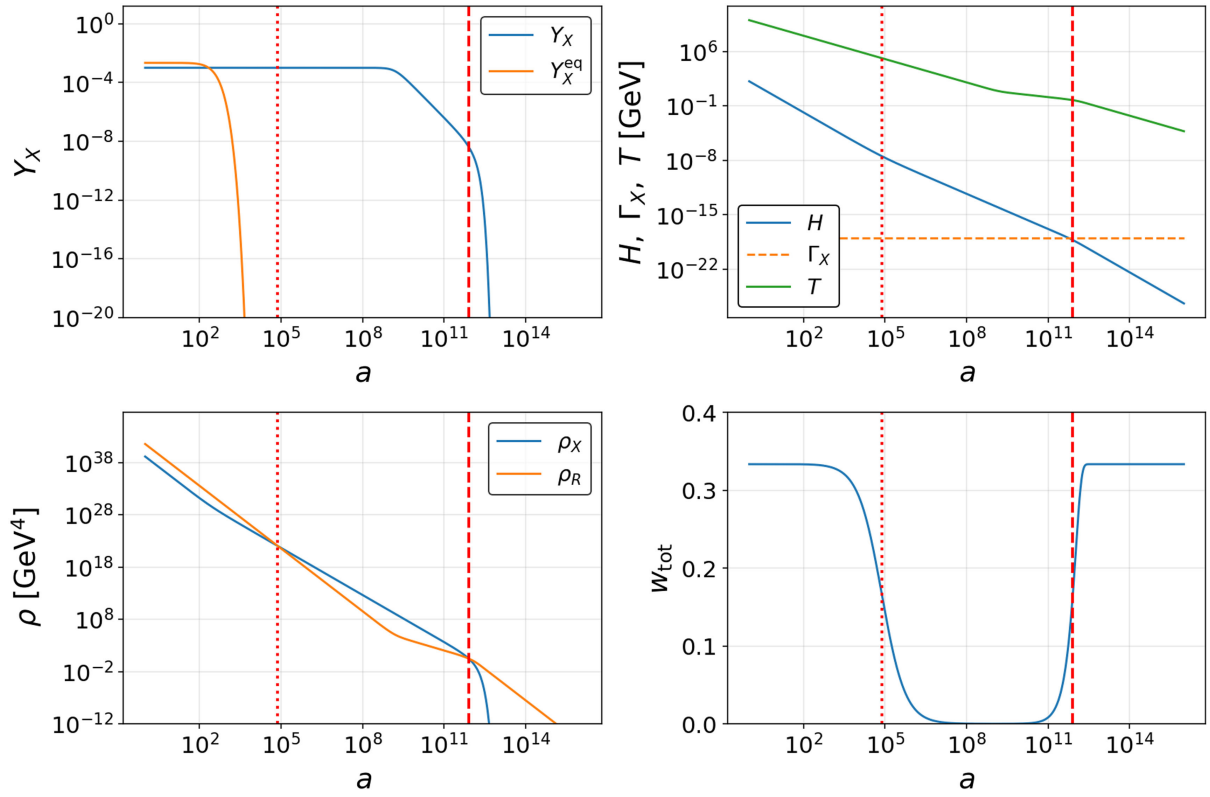


FIG. 1. Benchmark result for early matter domination by a heavy long-lived BSM particle. Plots show the evolution of the abundances (top left), the Hubble parameter and temperature (top right), the physical energy densities (bottom left) and the equation of state parameter (bottom right). The dotted and dashed red vertical lines mark the beginning and end of the early matter-dominated era, respectively. Parameters are $M_X = 10^8$ GeV, $Y_i = 10^{-3}\Gamma = 10^{-18}$ GeV. We fixed $g_X = 1$; however this is independent of the results. Discussion of results is given in the text.

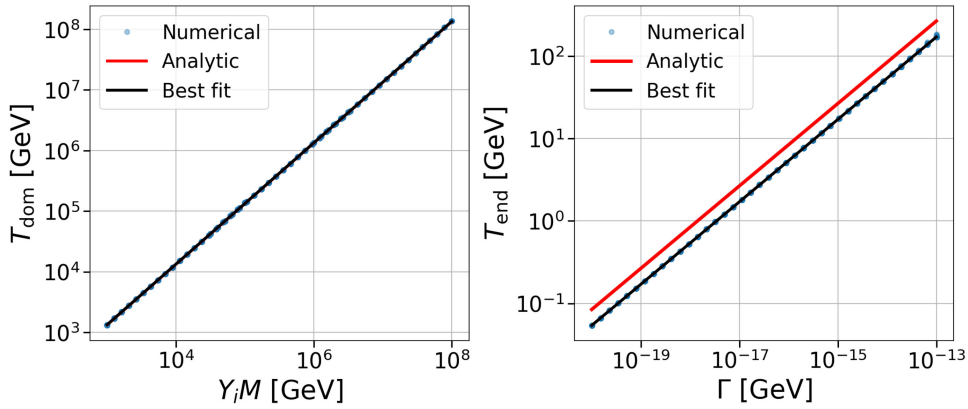


FIG. 2. Scan for early matter domination by a heavy long-lived BSM particle. Parameters $T_i = 100M$ and scanned over the Γ, M, Y_i parameter space. We fixed $g_X = 1$; however this is larger independent of the results as is the initial temperature so long as the species begins as relativistic. As with the analytical estimate the domination temperature is determined by the product of mass and initial abundance, and the final temperature is determined by the decay rate, however with slightly reduced prefactors. Further discussion is given in the text.

where $\tilde{m}$ is the effective neutrino mass. Taking $Y_i = 3.9 \times 10^{-3}$ and $v = 174$ GeV, the dependence on M cancels, and Eq. (15) becomes

$$\tilde{m} < 7.5 \times 10^{-8} \text{ eV}. \tag{17}$$

Although the cancellation of the heavy-neutrino mass is elegant, this condition requires a very small effective neutrino mass in the minimal model.

(2) Consider instead a massive scalar with $M_\phi = 10^{12}$ GeV and $Y_i = 10^{-1}$, decaying with

$$\Gamma_\phi = \frac{y^2}{8\pi} M_\phi. \tag{18}$$

Equation (15) then gives

$$y < 1.3 \times 10^{-3}. \tag{19}$$

This coupling is not especially small and is comparable to several Standard Model Yukawa couplings.

The right-handed-neutrino example therefore requires a strongly suppressed effective neutrino mass, whereas the scalar example can satisfy the condition with a comparatively ordinary coupling. Indeed, five of the nine charged-fermion Yukawa couplings in the Standard Model lie below the scalar benchmark bound. These examples demonstrate that an early matter-dominated era is a generic possibility for sufficiently long-lived particles with a non-negligible initial abundance, rather than a feature tied to a particular model. We now examine how this departure from radiation domination is imprinted on a gravitational-wave background.

III. GRAVITATIONAL WAVE BACKGROUNDS WITH EARLY MATTER DOMINATION

The quantity of interest is the gravitational wave background, defined as the fractional energy density in gravitational waves per logarithmic frequency interval,

$$\Omega_{\rm GW}(a, f) \equiv \frac{1}{\rho_{\rm tot}(a)} \frac{d\rho_{\rm GW}(a)}{d\ln f}, \tag{20}$$

where $\rho_{\rm GW}$ is the energy density of the gravitational wave background and f denotes the frequency. We first consider a GWB whose production has ceased before the EMD transfer is evaluated. The subsequent tensor evolution is homogeneous, so that the observed spectrum factorizes as

$$\Omega^{\rm obs}_{\rm GW}(f) = \mathcal{T}_{\rm EMD}(f)\Omega^{\rm ref}_{\rm GW}(f). \tag{21}$$

Here $\Omega^{\rm ref}_{\rm GW}$ is the spectrum propagated through a reference radiation-dominated history, and $\mathcal{T}_{\rm EMD}$ depends on the postproduction expansion history rather than on the microphysical production mechanism. We assume that there is a background GWB that has already been produced and is no longer being sourced and is freely propagating so that the only change is the cosmological evolution due to the change of the equation of state of the Universe. This scenario may arise in first-order phase transitions, domain walls [44], scalar induced [117] and inflationary gravitational wave backgrounds.

Each observed frequency corresponds to a particular gravitational-wave mode. This mode does not immediately behave as a radiation component after production. While its physical wavelength is larger than the Hubble radius, the tensor perturbation is effectively frozen and does not propagate as a wave. In this regime the usual radiationlike redshifting description is not applicable, and the gravitational-wave energy fraction is not well-defined. As the Universe expands, the Hubble radius grows relative to the wavelength, and the mode eventually enters the horizon when its physical scale becomes comparable to the Hubble scale. From this point onward the mode oscillates and propagates freely, redshifting like radiation. Therefore, the evolution of the gravitational-wave background begins only after horizon entry, and $\Omega_{\rm GW}$ evolves only once the corresponding mode is inside the horizon. Horizon entry occurs when the physical wave number becomes comparable to the Hubble scale. This transition from superhorizon to subhorizon evolution is defined by

$$k = a_{\rm ent} H(a_{\rm ent}), \qquad k = 2\pi f_0 a_0, \tag{22}$$

where the subscript "ent" indicates the horizon entry, f_0 is the frequency as measured today and a_0 is the scale factor measured today which we calculate from our Boltzmann code assuming that between the end of the Boltzmann evolution and today there are no non-negligible entropy dumps. Under this assumption, the present-day scale factor is given by

$$a_0 = a_f \frac{T_f}{T_0} \left(\frac{g_*(T_f)}{g_*(T_0)}\right)^{\frac{1}{3}} \tag{23}$$

where a_f is the final scale factor of the evolution of Boltzmann equations, T_f and T_0 are the final temperature of Boltzmann's and the temperature today respectively, and g_* is the degrees of freedom for the corresponding times.

This equation implicitly defines the entry scale factor for each frequency. In other words, the function $a_{\rm ent}(f)$ provides the mapping between frequency space and cosmic time: higher-frequency modes satisfy this condition at earlier times (smaller scale factor), while lower-frequency modes enter later.

From the equation of motion for the tensor modes, it follows that in the superhorizon regime the modes are frozen, and therefore do not feel the effects of an early matter-dominated phase. Once a mode is inside the horizon, the fluid equations governing the energy densities of the gravitational-wave background and the total energy content of the Universe are

$$\dot\rho_{\rm GW} + 4H\rho_{\rm GW} = 0, \quad \dot\rho_{\rm tot} + 3H(w(a)+1)\rho_{\rm tot} = 0. \tag{24}$$

Differentiating with respect to the e-fold variable $\ln a$, the gravitational-wave background $\Omega_{\rm GW}$ evolves as

$$\frac{d\ln\Omega_{\rm GW}}{d\ln a} = 3w(a) - 1. \tag{25}$$

We now integrate this equation to obtain the full evolution of the spectrum. Evolution starts at the horizon-entry scale

factor $a_{\rm ent}(f)$. We therefore integrate from this point to some later time after we return to radiation domination. Integrating both sides and exponentiation gives

$$\Omega_{\rm GW}(a_f, f) = \Omega_{\rm GW}^{\rm RD}(f) \mathrm{Exp}\left[\int_{\ln a_{\rm ent}(f)}^{\ln a_f} (3w(a) - 1) d\ln a\right], \tag{26}$$

where the superscript RD refers to the background under pure radiation domination. The above shows that there will be no departure from standard evolution during radiation domination $w = 1/3$. Then as we have a period of early matter domination where $w < 1/3$ there will be a suppression of the background before then returning the standard evolution predicted by radiation domination.

The analysis above relies on the instantaneous horizon entry approximation, where the tensor amplitude is assumed to remain constant for $k < aH$ and to immediately transition to radiationlike redshifting once $k > aH$. This is the correct result if the crossing occurs during radiation domination; however, if there is a deviation from radiation domination the modes will have an associated factor [36]. This factor is a well-known result dependent on the equation of state parameter evaluated at horizon entry:

$$C(w) = \frac{\Gamma^2(\alpha + \frac{1}{2})}{\pi} \left(\frac{2}{\alpha}\right)^{2\alpha}, \qquad \alpha = \frac{2}{1 + 3w}, \tag{27}$$

where α should be evaluated at horizon reentry, $k = aH$ assuming that w is roughly constant during the crossing.[2] As the return to radiation domination occurs from decays this is an accurate approximation.[3] This factor is therefore 1 for radiation domination, and early matter domination is $9/16$ so is an $\mathcal{O}(1)$ correction to the amplitude. We must also account for the effect of entropy injection on the source. Due to reheating, a given mode is mapped to an earlier effective emission time, resulting in a shift in the observed frequencies.[4] We distinguish the comoving entropy from the GW transfer function. Define

$$\mathcal{S}_{\rm com}(a) \equiv s(a) a^3, \qquad \Delta \equiv \frac{\mathcal{S}_{\rm com,f}}{\mathcal{S}_{\rm com,i}}. \tag{28}$$

If the reference source spectrum is tabulated as a function of a predecay frequency coordinate, entropy production induces the horizontal remapping $f \mapsto f\Delta^{1/3}$. The full result can then be written as

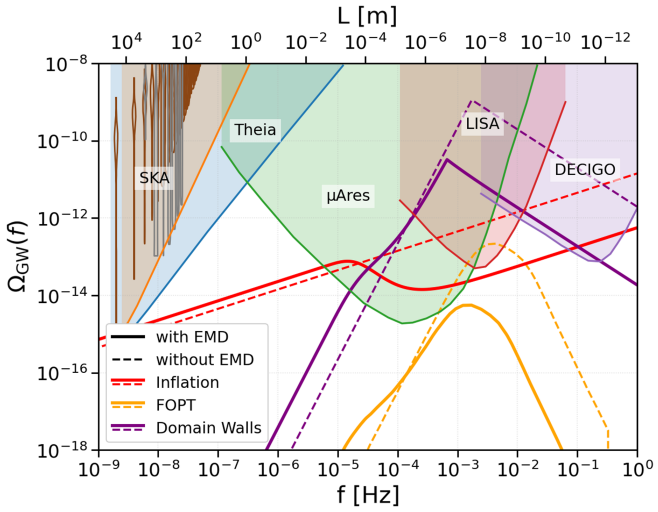


FIG. 3. Benchmark GWBs with (solid lines) and without (dashed lines) an early matter-dominated era. Results are shown for inflationary (red), first-order phase transitions (orange), and domain wall (purple). The shaded regions indicate the projected sensitivity of each detector, with the corresponding experiments labeled. Parameters for each benchmark are shown in Table II. The upper x axis indicates the location of the first feature for a particle with decay length L.

$$\Omega_{\rm GW}(a_f, f) = \Omega_{\rm GW}^{\rm RD}(f\Delta^{1/3}) \mathcal{T}_{\rm EMD}(f), \tag{29}$$

where

$$\mathcal{T}_{\rm EMD}(f) = C[w(a_{\rm ent})] \exp\left[\int_{\ln a_{\rm ent}(f)}^{\ln a_f} (3w(a) - 1) d\ln a\right]. \tag{30}$$

We can see that $\mathcal{T}_{\rm EMD}$ encodes both the thermal history of the Universe and the effects of the early matter-dominated era, and we examine this function in detail in the following sections.

A. Results

To showcase the wide applicability of this framework, we present Fig. 3 which displays gravitational-wave backgrounds from various sources with and without the subsequent period of early matter domination.[5] As demonstrated by these benchmarks, gravitational wave observations can resolve both the onset and termination of an early period of matter domination for each source showing a clear and obvious feature compared to the background without a period of early matter domination. However, first-order phase transitions illustrate a complementary effect: in this case, the resulting signal can mask these features, allowing such scenarios to evade detection and thereby reopen regions

[2]Γ in Eq. (27) denotes the gamma function, not the decay rate.
[3]Our analysis is valid if X decays solely into radiationlike particles. This could be visible or dark radiation.
[4]Should the source be fixed a certain time in the past with respect to the present, then this shift is not there; see [79,118,119].
[5]For the benchmarks in Fig. 3 we assume the GWB is sourced during radiation domination, and then a period of EMD occurs afterward.

TABLE II. Benchmark parameters for each gravitational-wave source shown in Fig. 3. The inflationary benchmark adopts a tensor power-law spectrum with the corresponding radiation-era transfer function, following Refs. [120–122]. The annihilating-domain-wall benchmark is described using the standard broken-power-law parametrization of the peak spectrum from Refs. [123,124], with plasma-friction effects neglected. For the first-order phase-transition benchmark, we include the sound-wave contribution using the numerical implementation of Ref. [125], based on the treatment of Ref. [126]. The specific production mechanism of the gravitational-wave background does not affect the particle-physics information extracted from the spectrum, since the two characteristic frequencies occur at the same locations for all freely propagating GWBs.

Source	Parameters
Inflation	$\epsilon_{\rm inf} = 5 \times 10^{-5}, n_T = 0.5$
FOPT	$\alpha = 0.25$, $\beta/H = 50$, $T_n = 1000$ GeV, $v_w = 1$
Domain walls	$\sigma_t = 2 \times 10^{17}$ GeV, $\mathrm{V_t} = 6 \times 10^{28}$ GeV, $\epsilon = 0.7$, $\mathrm{A} = 0.8$
LLP	$\Gamma = 10^{-12}$ GeV, $M = 10^6$ GeV, $Y_i = 0.01$, $MY_i = 10^4$

of parameter space previously thought to be excluded. The purpose of Fig. 3 is to demonstrate that the same post-production transfer function acts on distinct transient source shapes, not to rederive standard source spectra. The inflationary benchmark uses the tensor power-law spectrum and its radiation-era transfer as in Refs. [120–122]. The annihilating-domain-wall benchmark uses the standard broken-power-law peak parametrization of Refs. [123,124], neglecting plasma friction. The first-order phase-transition benchmark includes the sound-wave contribution evaluated with the numerical implementation of Ref. [125], based on Ref. [126]. Their parameters are listed in Table II. Since these expressions are standard and enter only through the reference spectrum $\Omega^{\rm ref}_{\rm GW}(f)$ in Eq. (21), we do not reproduce their derivations here. We now find the relationship between our initial parameters (Y_i, M, Γ) and map to our transfer function as this is the key quantity that determines the GWB spectral features defined as

$$\mathcal{T}_{\rm EMD} = C(w)\mathrm{Exp}\left[\int_{\ln a_{\rm ent}(f)}^{\ln a_f} (3w(a) - 1) d\ln a\right]. \quad (31)$$

The constant radiation domination corresponds to $\mathcal{T}_{\rm EMD} = 1$. In the radiation-dominated regime at both early and late times, $w = \frac{1}{3}$, so the exponent vanishes and $\mathcal{T}_{\rm EMD}$ remains constant, resulting in two flat plateaus. During an ideal matter-dominated interval, $w = 0$, and Eq. (30) gives

$$\mathcal{T}_{\rm EMD} \simeq 0.6\,\mathrm{Exp}\left[\int_{\ln a_{\rm ent}(f)}^{\ln a_f} (-1) d\ln a\right] = \mathcal{O}(1)\frac{a_{\rm ent}}{a_f}. \quad (32)$$

During early matter domination we have, $k = a_{\rm ent}H(a_{\rm ent})$, $H \propto a^{-3/2}$; therefore we have, $a_{\rm ent} \propto f^{-2}$ meaning $\mathcal{T}_{\rm EMD} \propto f^{-2}$ during early matter domination. To model this behavior we fit the numerical results using the smooth broken power-law form,[6]

$$\mathcal{T}^{\rm fit}_{\rm EMD}(f) = \frac{1 + (f/f_2)^2}{1 + (f/f_1)^2}, \qquad f_1 < f_2. \quad (33)$$

The three asymptotic regimes are

$$\mathcal{T}^{\rm fit}_{\rm EMD}(f) \simeq \begin{cases} 1, & f \ll f_1, \\ (f_1/f)^2, & f_1 \ll f \ll f_2, \\ (f_1/f_2)^2, & f \gg f_2. \end{cases} \quad (34)$$

Thus the intermediate branch has the expected f^{-2} scaling, while the high-frequency modes form a fully suppressed plateau. The fitted f_1 and f_2 are template parameters extracted from the smooth spectrum; they are associated with, but need not be numerically identical to, instantaneous horizon scales evaluated at the density crossings. The frequency $f_1(f_2)$ corresponds to modes entering the horizon near the end (start) of the early matter-dominated era. Modes with $f < f_1$ enter after radiation domination resumes and therefore remain unaffected. Modes with $f > f_2$ are already subhorizon before the deviation from radiation domination and thus experience the full suppression. These two frequencies are the GWB observables of interest as described in Fig. 5. These frequencies corresponding to the start and end of early matter domination therefore we will relate them to our initial parameters MY_i and Γ.

We numerically solve the Boltzmann equations to obtain $w(a)$ for each case, then solve Eq. (30) and fit to Eq. (33) to determine the dependence of the characteristic frequencies on the decay rate, initial abundance, and mass of the particle. The validity of these fits and more details are provided in Sec. B. The results of this scan are shown in Fig. 4.

We found f_1 depends solely on the decay rate. By contrast f_2 has strong dependence on the product Y_iM; however when redshifting the frequency to the present there is a slight dependence on the length of early matter domination that occurred giving a slight dependence on the decay rate. This comes from the entropy dump at the end of the early matter domination period. The scan for f_1 yields the best-fit relation,

$$f_1 = 20.6\left(\frac{\Gamma}{\rm GeV}\right)^{1/2} \mathrm{Hz}, \quad (35)$$

while the scan for f_2 gives the best-fit relation:

$$f_2 = 2.77 \times 10^{-5}\left(\frac{Y_iM}{\rm GeV}\right)^{2/3}\left(\frac{\Gamma}{\rm GeV}\right)^{1/6} \mathrm{Hz}. \quad (36)$$

[6]The validity of this fit is discussed in Appendix B.

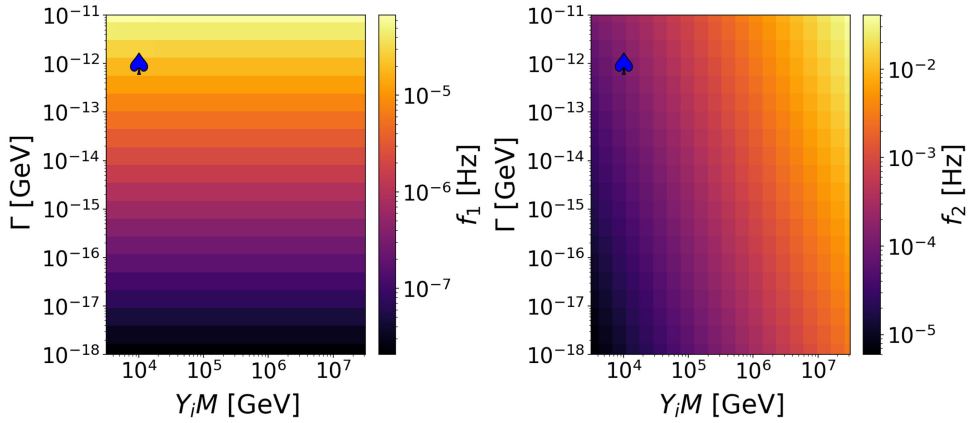


FIG. 4. Scan of the characteristic frequencies over decay rate and product of mass and initial abundance recording the frequencies of the best fit parameters. We can see that f_1 is solely dependent on the decay rate corresponding to the end of early matter domination and that f_2 has a main dependence on Y_iM and a mild dependence on the decay rate. The benchmark used in Fig. 3 is denoted by the blue spade. Further discussion is given in the text.

Once a model has been specified the Lagrangian parameters can be determined by specifying the initial abundance and writing the decay rate in terms of the mass and Lagrangian couplings. These best-fit expressions are not universally valid. The fit for f_1 remains accurate up to the bound given in Eq. (15) and can be used in future analysis. In contrast, the fit for f_2 is only reliable for decay rates at least 2 orders of magnitude below this bound. This can be understood from the fact that the best-fit result assumes a fully matter-dominated phase with $w = 0$. However, for short periods of early matter domination, such as those arising for decay rates close to the boundary of Eq. (15), the equation of state never truly reaches $w = 0$. Achieving this would require $\rho_X \gg \rho_R$, whereas in this regime one typically has only $\rho_X > \rho_R$. As a result, the system remains in a partially matter-dominated phase, and the idealized scaling underlying the best fit is no longer valid. In Appendix A, we derive this scaling, finding agreement up to a differing overall prefactor.

To make the complementarity with collider searches for LLPs more transparent, we rewrite the characteristic frequency f_1 in terms of the proper decay length, $L = 1/\Gamma$, in meters,

$$f_1 = 2.9 \times 10^{-7} \left(\frac{1\ \mathrm{m}}{L}\right)^{1/2} \mathrm{Hz}. \tag{37}$$

This is shown in Fig. 3 as the top x axes. As a representative example, particles with decay lengths of order $L \sim \mathcal{O}(100)$ m which is accessible in MATHUSLA [91,127] correspond to a frequency $f_1 \simeq 2 \times 10^{-8}$ Hz, placing the signal squarely within the sensitivity range of pulsar timing array experiments, [27,28,32,33], as well as future facilities such as SKA [24–26] and Theia [23].[7]

[7]For earlier estimates in the context of right-handed neutrinos, see [79].

TABLE III. Mapping between gravitational wave frequency f_1 and decay length L using $L = 1\ \mathrm{m}[(2.9 \times 10^{-7}\ \mathrm{Hz})/f_1]^2$. Lower frequencies correspond to larger decay lengths, while higher-frequency detectors probe increasingly microscopic scales.

Detector	Frequency f_1 (Hz)	Decay length L (m)
Theia/SKA	$10^{-9} - 10^{-7}$	$10^{5} - 10^{1}$
μAres/LISA	$10^{-6} - 10^{-2}$	$10^{-1} - 10^{-9}$
DECIGO	$10^{-2} - 1$	$10^{-9} - 10^{-13}$
ET/CE	$1 - 10^{2}$	$10^{-13} - 10^{-17}$

Remarkably, this frequency lies in the region where a stochastic gravitational-wave background has recently been reported by NANOGrav, suggesting that LLP scenarios with decay lengths accessible at colliders could leave observable imprints in the nano-hertz gravitational-wave spectrum. It is worth emphasizing that any parameter space satisfying Eq. (15) will produce a feature at the frequency given by Eq. (37). Importantly, this means that Eq. (37) can generally be used. To show what decay lengths are then probed by each future experiment we provide Table III. We can see that due to the large range of frequencies being probed by upcoming experiments a large range of particle decay lengths are being probed. Once a specific particle physics model is specified, these frequencies can be mapped onto Lagrangian parameters, such as the particle mass and coupling constants through the decay rate. The general process of deducing the Lagrangian parameters from the gravitational wave observables is shown in Fig. 5.[8]

[8]A recent follow-up to an earlier version of this work [54] showed that, for gravitinos and more generally for particles whose decay is gravitationally suppressed, the first break frequency f_1 maps directly onto the mass of the BSM particle. This illustrates that some classes of BSM particles can encode more detailed information in the gravitational-wave spectrum than others.

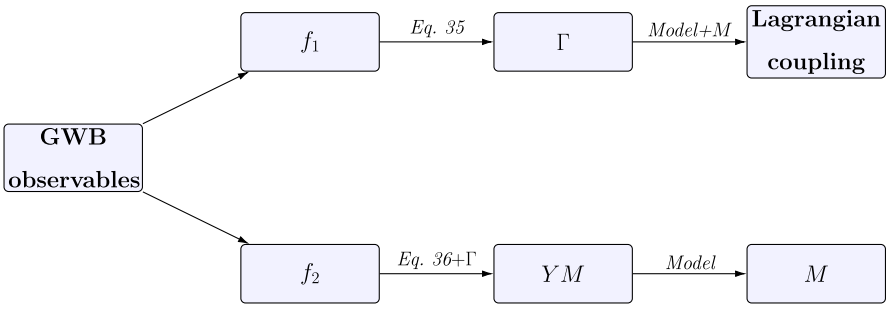


FIG. 5. Schematic showing how gravitational-wave-background observables can be mapped onto particle-physics parameters. The characteristic frequency f_1, associated with the end of early matter domination, determines the decay rate Γ through Eq. (35). For a freely propagating GWB, the characteristic frequency f_2, associated with the onset of early matter domination, determines the product $Y_i M$ through Eq. (36) once Γ is known. Separating $Y_i M$ into the particle mass M and initial abundance Y_i, and relating Γ to an underlying Lagrangian coupling, require specification of the particle model and production mechanism.

B. Nontransient and sourced GWBs

We now consider gravitational-wave backgrounds that remain actively sourced during the early matter-dominated era. In this case the gravitational-wave fluid equation is modified by the addition of a source term,

$$\dot{\rho}_{\rm GW}(t,f) + 4H(t)\rho_{\rm GW}(t,f) = \mathcal{S}(t,f), \tag{38}$$

where $\mathcal{S}(t,f)$ denotes the gravitational-wave energy injected per unit time and per logarithmic frequency interval. Following the logic of the last section we obtain

$$\frac{d\Omega_{\rm GW}(a,f)}{d\ln a} = (3w(a)-1)\Omega_{\rm GW}(a,f) + \frac{\mathcal{S}(a,f)}{H(a)\rho_{\rm tot}(a)}. \tag{39}$$

Defining

$$\mathcal{J}(a,f) \equiv \frac{\mathcal{S}(a,f)}{H(a)\rho_{\rm tot}(a)}, \tag{40}$$

the solution at a final scale factor a_f is

$$\Omega_{\rm GW}(a_f,f) = \Omega_{\rm GW}(a_i,f)\exp\left[\int_{\ln a_i}^{\ln a_f}(3w(a)-1)d\ln a\right] + \int_{\ln a_i}^{\ln a_f} d\ln a'\,\mathcal{J}(a',f)\exp\left[\int_{\ln a'}^{\ln a_f}(3w(a)-1)d\ln a\right]. \tag{41}$$

The first term is the freely propagating contribution considered previously, while the second term contains gravitational waves continuously generated at different times. Each contribution produced at a' is therefore multiplied by the transfer factor

$$\mathcal{T}(a',a_f) \equiv \exp\left[\int_{\ln a'}^{\ln a_f}(3w(a)-1)d\ln a\right]. \tag{42}$$

The lower-frequency feature f_1 corresponds to the comoving Hubble scale at the end of early matter domination,

$$f_1 = \frac{a_{\rm end}H_{\rm end}}{2\pi a_0}. \tag{43}$$

At $a = a_{\rm end}$, the equation of state returns to radiation domination, $w = 1/3$, and hence the dilution term in Eq. (39) vanishes. This transition occurs at the same background time irrespective of whether the gravitational-wave background is freely propagating or continuously sourced. The position of the feature is therefore unchanged:

$$f_1^{\rm sourced} = f_1^{\rm transient} = \frac{a_{\rm end}H_{\rm end}}{2\pi a_0}. \tag{44}$$

Consequently, the relation between f_1 and the decay rate remains valid,

$$f_1 = 20.6\left(\frac{\Gamma}{\rm GeV}\right)^{1/2}\ {\rm Hz}. \tag{45}$$

We note, however, that a source-dependent spectral structure may partially mask or mimic the EMD-induced feature, introducing a degeneracy in its observational identification even though its underlying cosmological scale remains fixed.

The situation is different for the second characteristic frequency. For a transient background, f_2 is associated with the comoving Hubble scale at the onset of early matter domination,

$$f_2^{\text{transient}} = \frac{a_{\text{dom}} H_{\text{dom}}}{2\pi a_0}. \quad (46)$$

All modes with $f > f_2$ are already inside the horizon before matter domination begins and therefore experience the complete suppression. For an actively sourced background, however, gravitational waves at a fixed observed frequency can be generated both before and during early matter domination. Equation (41) then gives

$$\Omega_{\text{GW}}^{\text{sourced}}(a_f, f) = \int_{\ln a_i}^{\ln a_f} d\ln a' \mathcal{J}(a', f)\mathcal{T}(a', a_f), \quad (47)$$

up to any preexisting freely propagating contribution. The observed spectrum is thus a convolution of the time-dependent source with the cosmological transfer function. The location and shape of the feature associated with the onset of matter domination consequently depend on the time and frequency dependence of $\mathcal{S}(a, f)$ and in general, $f_2^{\text{sourced}} \neq f_2^{\text{transient}}$. We therefore conclude that for a non-transient gravitational-wave background the frequency f_1 remains a source-independent probe of the end of early matter domination and hence of the decay rate Γ. By contrast, f_2 depends on the detailed evolution of the gravitational-wave source, so the extraction of $Y_i M$ becomes source dependent.

IV. DISCUSSION AND CONCLUSION

A sufficiently long-lived particle can generate a temporary epoch of EMD, leaving a characteristic imprint on a stochastic gravitational-wave background. For a pre-existing, freely propagating GWB whose source has switched off, the effect of EMD factorizes into the reference spectrum and an EMD transfer function. The two characteristic break frequencies then determine the cosmological combinations

$$(f_1, f_2) \longrightarrow (\Gamma, Y_i M), \quad (48)$$

through Eqs. (35) and (36). Recovering the individual particle parameters requires additional microscopic input: separating $Y_i M$ into the abundance Y_i and mass M requires a specified production history, while relating Γ to a coupling depends on the particle model. Under these assumptions, the measured spectral features can be translated into particle masses and couplings, as illustrated by our right-handed-neutrino and scalar examples. The corresponding precision therefore inherits both the observational uncertainty in the reconstructed break frequencies and the theoretical uncertainty associated with the production mechanism.

For actively sourced backgrounds, the situation is less universal. The EMD epoch still defines the cosmological scales f_{end} and f_{dom}, with $f_{\text{end}} \propto \Gamma^{1/2}$ fixed by the end of matter domination. However, because the observed spectrum is determined by the convolution in Eq. (47), the visibility and precise fitted location of these features can depend on the source history. In particular, the reconstruction of $Y_i M$ from the second scale is generally source dependent, whereas the decay-rate information associated with f_{end} remains considerably more robust. The EMD condition in Eq. (15) also favors increasingly heavy particles, allowing gravitational-wave observations to probe masses far beyond those directly accessible at terrestrial experiments.

We considered decay rates relevant for future long-lived-particle searches at experiments such as DUNE [88], MATHUSLA [91], and SHiP [94]. Remarkably, we found that the corresponding decay lengths map directly onto the nanohertz frequency range in which NANOGrav has reported evidence for a stochastic gravitational-wave background. At the same time, gravitational-wave observations extend sensitivity to particle masses far beyond the reach of terrestrial colliders. Future detections of stochastic gravitational-wave backgrounds may therefore reveal otherwise inaccessible information about long-lived particles and nonstandard epochs in the thermal history of the Universe, establishing a direct complementarity between pulsar timing arrays, future gravitational-wave observatories, and laboratory searches for long-lived particles.

We are now entering an era in which gravitational-wave observatories can double as particle detectors.

ACKNOWLEDGMENTS

The authors thank Germano Nardini, Pankaj Borah, Nimmala Narendra, Shuailiang Ge, Elliot Tole and Yuhsin Tsai for useful discussions and comments on the manuscript. The authors are indebted to Marek Lewicki for pointing out an inaccuracy in Eq. (29) in version 1, which consequently affected Fig. 3. The key results of this work. Eq. (35) and Eq. (36), were not affected. G. W. and A. S. acknowledge the STFC Consolidated Grant No. ST/X000583/1. A. S. thanks the University of Southampton School of Physics and Astronomy for the support of a Mayflower PhD scholarship. A. G. acknowledges the support from the Royal Society, UK, Funding Reference No. NIF R1 253963.

DATA AVAILABILITY

There are no publicly available research data or software supporting this manuscript. Requests for further information or data should be sent to the authors.

APPENDIX A: BREAKING FREQUENCY DEPENDENCE

In this section, we derive analytic approximations for the two characteristic frequencies, which serve as our key observables. We recover the correct scaling with the input parameters Γ, M, Y_i, albeit with a slightly different numerical prefactor.

The first frequency f_1 from the plot is solely determined by the decay rate; we now provide a calculation showing this dependence. The frequency can be determined from the comoving horizon scale at the end of early matter domination redshifted to today,

$$f_1 = \frac{a_{\rm end} H_{\rm end}}{2\pi a_0}. \tag{A1}$$

Approximating $H_{\rm end} \simeq \Gamma$ and using entropy conservation,

$$\frac{a_{\rm end}}{a_0} = \frac{T_0}{T_{\rm end}} \left(\frac{g_{*s,0}}{g_{*s}}\right)^{1/3} \simeq 0.34 \frac{T_0}{T_{\rm end}}, \tag{A2}$$

where we used $g_{*s,0} = 3.91$ and $g_{*s} = 106.75$. Using the relation $T_{\rm end} = 0.15\sqrt{\Gamma M_{\rm Pl}}$, this gives

$$f_1 = \frac{T_0}{2\pi \cdot 0.15} \left(\frac{g_{*s,0}}{g_{*s}}\right)^{1/3} \frac{\Gamma^{1/2}}{\sqrt{M_{\rm Pl}}} \simeq 36.0 \left(\frac{\Gamma}{\rm GeV}\right)^{1/2} \text{Hz}, \tag{A3}$$

which is the scaling observed in the numerical scans, with the overall normalization differing by a factor of $\mathcal{O}(1.5)$. This discrepancy arises from the simplifying assumption of an instantaneous decay, $H_{\rm end} \simeq \Gamma$.

Now we evaluate f_2, the frequency corresponding to the onset of early matter domination. Using the horizon-entry condition $k = aH$, the observed frequency today scales as

$$f(a_{\rm ent}) = \frac{k}{2\pi a_0} = \frac{a_{\rm ent} H(a_{\rm ent})}{2\pi a_0}. \tag{A4}$$

It is convenient to consider the ratio of the two characteristic frequencies,

$$\frac{f_2}{f_1} = \frac{a_{\rm dom} H_{\rm dom}}{a_{\rm end} H_{\rm end}}. \tag{A5}$$

During the early matter-dominated era the Hubble rate scales as $H \propto a^{-3/2}$, giving

$$\frac{f_2}{f_1} = \left(\frac{a_{\rm end}}{a_{\rm dom}}\right)^{1/2} = \left(\frac{\rho_{\rm dom}}{\rho_{\rm end}}\right)^{1/6}. \tag{A6}$$

At the onset of early matter domination $\rho_X = \rho_R$, so that

$$\rho_{\rm dom} = 2\rho_R = \frac{\pi^2}{15} g_* T_{\rm dom}^4. \tag{A7}$$

At the end of early matter domination, using $H_{\rm end} \simeq \Gamma$ and the Friedmann equation,

$$\rho_{\rm end} = \frac{3 M_{\rm Pl}^2 \Gamma^2}{8\pi}. \tag{A8}$$

Combining these gives

$$\frac{f_2}{f_1} = \left(\frac{8\pi^3 g_*}{45}\right)^{1/6} T_{\rm dom}^{2/3} M_{\rm Pl}^{-1/3} \Gamma^{-1/3}. \tag{A9}$$

Using $T_{\rm dom} = \frac{4}{3} Y_i M$, we obtain

$$f_2 = f_1 \left(\frac{8\pi^3 g_*}{45}\right)^{1/6} \left(\frac{4}{3} Y_i M\right)^{2/3} M_{\rm Pl}^{-1/3} \Gamma^{-1/3}. \tag{A10}$$

Substituting the analytic expression for f_1 then gives

$$f_2 = 5.5 \times 10^{-5} \left(\frac{Y_i M}{\rm GeV}\right)^{2/3} \left(\frac{\Gamma}{\rm GeV}\right)^{1/6} \text{Hz}. \tag{A11}$$

Once again we have derived the true scaling found by the Boltzmann evolution, however with a slightly different constant.

APPENDIX B: VALIDITY OF BEST FITS

In this section we assess the validity of the best-fit relations given in Eqs. (35) and (36) of the main text. As a quantitative validation, we compute the logarithmic coefficient of determination for each benchmark,

$$R^2_{\rm log} = 1 - \frac{\sum_i [\log_{10}\mathcal{T}_i - \log_{10}\mathcal{T}_{{\rm fit},i}]^2}{\sum_i [\log_{10}\mathcal{T}_i - \langle \log_{10}\mathcal{T}\rangle]^2}, \tag{B1}$$

which measures the quality of the fit in log space. We find $R^2_{\rm log} > 0.998$ throughout the scan, demonstrating that the template provides an excellent description of the numerical spectrum across the full frequency range. As a benchmark we provide Fig. 6. We now examine the validity of the extracted scaling relations for f_1 and f_2. Scanning over the parameter space, we find that the best-fit relation for f_1 remains robust provided the condition in Eq. (15) of the main text is satisfied. In contrast, the relation for f_2 in Eq. (36) of the main text breaks down when the duration of the early matter-dominated phase becomes too short. To illustrate this, we perform scans over increasing values of Γ, approaching the boundary of Eq. (15) of the main text, as shown in Fig. 7. Near this boundary, the numerical values of f_2 deviate systematically from the best-fit scaling, and only recover the expected behavior once Γ is at least 2 orders of magnitude below the maximum value allowing early matter domination.

This behavior has a clear physical origin. The derivation of the f_2 scaling assumes a well-defined matter-dominated phase with $w \simeq 0$. However, close to the boundary, the energy densities satisfy $\rho_M \sim \rho_R$, corresponding to an effective equation of state $w \simeq 1/6$, rather than $w = 0$. As a result, the system never fully enters a matter-dominated regime, invalidating the assumptions underlying the analytic scaling. To show this we take various scans

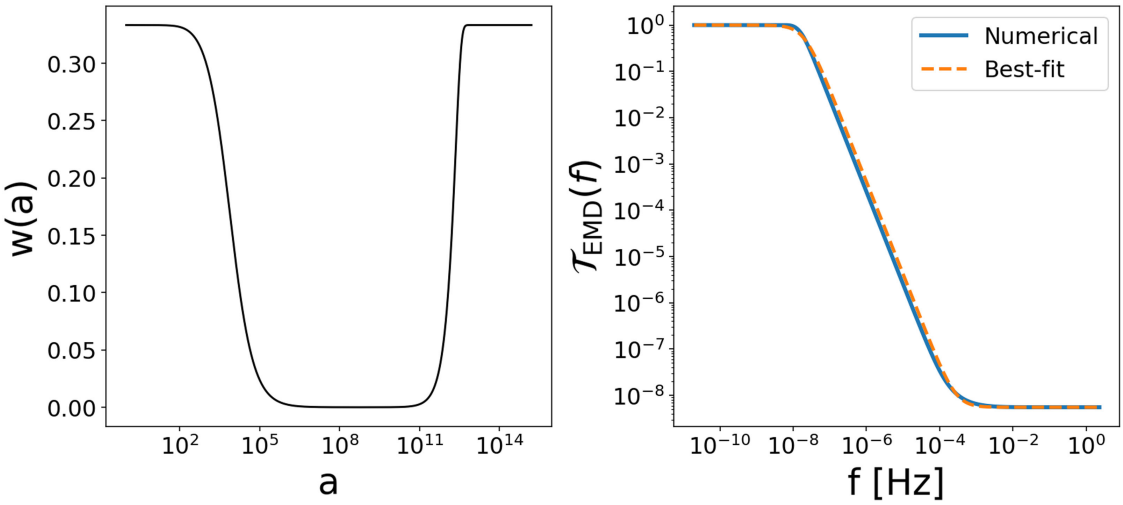


FIG. 6. Benchmark evolution of the dilution factor $\mathcal{T}_{\rm EMD}$ in Eq. (30) of the main text for the initial parameters $Y_i = 10^{-2}$, $M = 10^6$ GeV, and $\Gamma = 10^{-18}$ GeV. Left panel: evolution of the equation-of-state parameter. Right panel: numerical evaluation of the dilution factor $\mathcal{T}_{\rm EMD}(f)$ as a function of frequency together with the corresponding best-fit function, demonstrating excellent agreement between the numerical result and the fit.

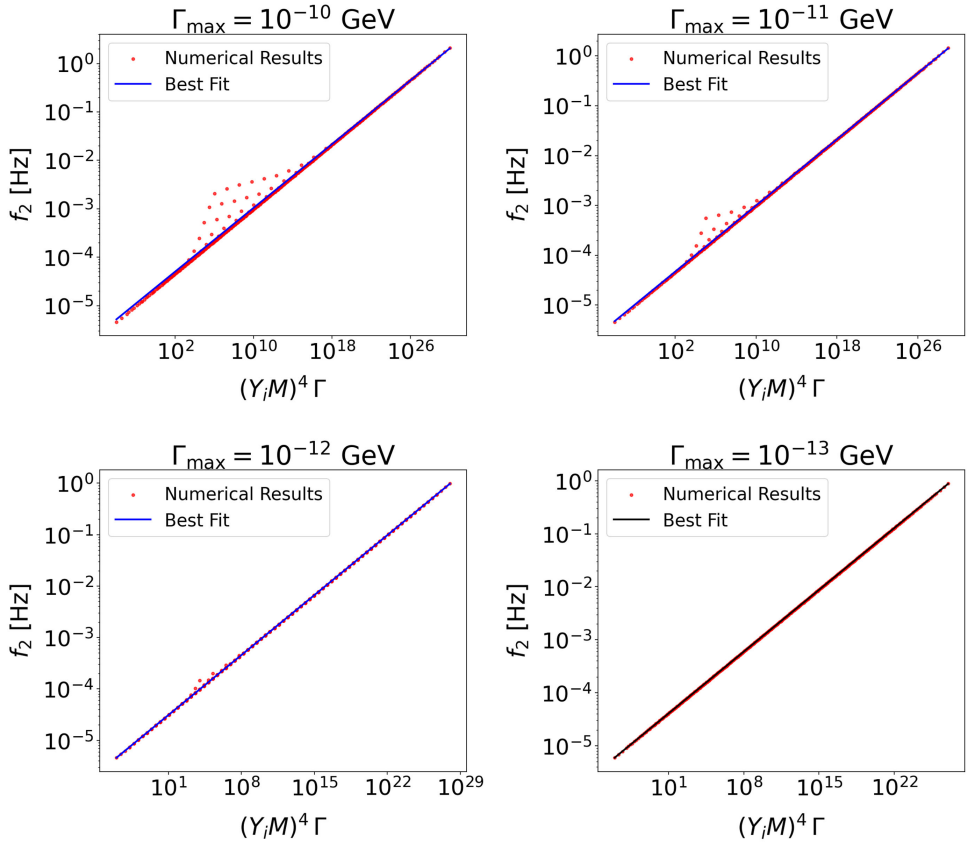


FIG. 7. Scan of f_2 for different maximum decay rates $\Gamma = 10^{-10}, 10^{-11}, 10^{-12}, 10^{-13}$ (ordered left to right, top to bottom). The maximum Γ that gives early matter domination is approximately $\Gamma_{\rm max} = 10^{-10}$ GeV. We can see that values of gamma close to this bound do not lie on the best fit line; it is not until 2 orders of magnitude below that this can be seen as a good fit.

over gamma up to approaching the boundary. We find that the best-fit relation becomes valid when the decay rate is approximately two orders of magnitude below the maximum value allowed by Eq. (15); for smaller decay rates, the best-fit relation remains unchanged. For the f_1 best fit, one should be able to reproduce the fit by scanning

from the boundary in Eq. (15) of the main text and to smaller decay rates. Therefore f_1 and as such the equation for decay length, Eq. (37) of the main text, are valid. This is due to the need for the best fit to achieve a $w = 0$ which does not happen for early matter domination close to the boundary as this is $\rho_M \approx \rho_R$ corresponding to a $w \approx \frac{1}{6}$ not 0.

APPENDIX C: REDSHIFTING VS ENTROPY DILUTION DISCUSSION

The suppression of a gravitational-wave background during a period of EMD is often described in terms of entropy dilution. However, this suppression may equivalently be understood directly from the modified redshifting behavior during the nonstandard expansion history. In this section we clarify that these are not distinct physical effects, but rather two equivalent interpretations of the same underlying dynamics caused by the dominant component of the energy budget.

The observable used for gravitational wave backgrounds is

$$\Omega_{\rm GW}(a,f) \equiv \frac{1}{\rho_{\rm tot}(a)} \frac{d\rho_{\rm GW}(a)}{d\ln f}, \tag{C1}$$

where we have used the conventional notation in the literature, $\rho_{\rm tot} = \rho_C$, after the inflationary phase. In this context, the two quantities are equivalent. The effect of early matter domination is twofold:

(1) Horizontal shift: Due to entropy injection increasing the temperature, modes undergo additional redshifting before reaching the present-day temperature.
(2) Vertical shift for some frequencies: Dilution due to the modified expansion history changing the evolution of ρ_C. This may be described in two equivalent ways:
   (a) The redshifting of ρ_C: ρ_C redshifts slower than $\rho_{\rm GW}$, leading to a suppression of the overall spectrum.
   (b) Entropy injection: After the EMD period has ended, the value of $\rho_{\rm tot}$ is larger than it would have been under uninterrupted radiation domination due to the entropy dump. This increases the background energy density relative to $\rho_{\rm GW}$, leading to a dilution of the gravitational-wave background.

We now look to show these are equivalent. We begin with the interpretation used in our analysis. For modes experiencing the full suppression plateau, we take the large frequency limit of our best fit, Eq. (34), of the main text:

$$\mathcal{T}_{\rm EMD}(f \gg f_2) = \frac{f_1^2}{f_2^2}. \tag{C2}$$

Using the scaling found for the characteristic frequencies,

$$f_1 \propto \Gamma^{1/2}, \qquad f_2 \propto (Y_i M)^{2/3}\Gamma^{1/6}, \tag{C3}$$

gives

$$\mathcal{T}^{\rm max}_{\rm EMD} \propto \Gamma^{2/3}(Y_i M)^{-4/3}. \tag{C4}$$

Thus the suppression becomes larger for longer periods of matter domination, corresponding to smaller decay rates or larger initial abundances. The same result may alternatively be derived from the entropy dilution picture. During reheating, the decay of the dominant matter component injects entropy into the thermal bath. Let us define the comoving entropy increase as [44]

$$\Delta \equiv \frac{S_f}{S_i} = \frac{s_f a_f^3}{s_i a_i^3} \simeq \frac{T_{\rm dom}}{T_{\rm end}}. \tag{C5}$$

The fractional gravitational-wave energy density is diluted according to [44]

$$\Omega_{\rm GW} \to \Omega_{\rm GW}\Delta^{-4/3}. \tag{C6}$$

Using

$$T_{\rm dom} \sim Y_i M, \qquad T_{\rm end} \sim \sqrt{\Gamma M_{\rm Pl}}, \tag{C7}$$

we obtain

$$\Delta^{-4/3} \sim \left(\frac{T_{\rm end}}{T_{\rm dom}}\right)^{4/3} \propto \Gamma^{2/3}(Y_i M)^{-4/3}, \tag{C8}$$

which reproduces precisely the same scaling obtained from the redshifting derivation.

We therefore conclude that the suppression of the gravitational-wave background is fundamentally caused by the modified expansion history during EMD through its impact on ρ_C. This effect may be interpreted either as the differential redshifting between $\rho_{\rm GW}$ and the dominant matter component ρ_C, or equivalently as entropy dilution during reheating. These are simply two complementary descriptions of the same physical process.

[1] C. Caprini and D. G. Figueroa, Classical Quantum Gravity **35**, 163001 (2018).
[2] P. Binétruy, A. Bohé, C. Caprini, and J.-F. Dufaux, J. Cosmol. Astropart. Phys. 06 (2012) 027.
[3] R. Roshan and G. White, Rev. Mod. Phys. **97**, 015001 (2025).
[4] N. van Remortel, K. Janssens, and K. Turbang, Prog. Part. Nucl. Phys. **128**, 104003 (2023).
[5] N. Christensen, Rep. Prog. Phys. **82**, 016903 (2018).
[6] B. P. Abbott *et al.* (LIGO Scientific Collaboration and Virgo Collaboration), Phys. Rev. Lett. **116**, 061102 (2016).
[7] B. P. Abbott *et al.* (LIGO Scientific Collaboration and Virgo Collaboration), Phys. Rev. Lett. **116**, 241103 (2016).
[8] B. P. Abbott *et al.* (LIGO Scientific Collaboration and Virgo Collaboration), Phys. Rev. Lett. **118**, 221101 (2017); **121**, 129901(E) (2018).
[9] B. . P.Abbott *et al.* (LIGO Scientific Collaboration and Virgo Collaboration), Astrophys. J. Lett. **851**, L35 (2017).
[10] B. P. Abbott *et al.* (LIGO Scientific Collaboration and Virgo Collaboration), Phys. Rev. Lett. **119**, 141101 (2017).
[11] B. P. Abbott *et al.* (LIGO Scientific Collaboration and Virgo Collaboration), Phys. Rev. Lett. **119**, 161101 (2017).
[12] L. Badurina, O. Buchmueller, J. Ellis, M. Lewicki, C. McCabe, and V. Vaskonen, Phil. Trans. R. Soc. A **380**, 20210060 (2021).
[13] P. W. Graham, J. M. Hogan, M. A. Kasevich, and S. Rajendran, Phys. Rev. D **94**, 104022 (2016).
[14] P. W. Graham, J. M. Hogan, M. A. Kasevich, S. Rajendran, and R. W. Romani (MAGIS Collaboration), arXiv:1711.02225.
[15] L. Badurina *et al.*, J. Cosmol. Astropart. Phys. 05 (2020) 011.
[16] M. Punturo *et al.*, Classical Quantum Gravity **27**, 194002 (2010).
[17] S. Hild *et al.*, Classical Quantum Gravity **28**, 094013 (2011).
[18] B. P. Abbott *et al.* (LIGO Scientific Collaboration), Classical Quantum Gravity **34**, 044001 (2017).
[19] D. Reitze *et al.*, Bull. Am. Astron. Soc. **51**, 035 (2019), arXiv:1907.04833
[20] J. Baker *et al.*, arXiv:1907.06482.
[21] Y. A. El-Neaj *et al.* (AEDGE Collaboration), Eur. Phys. J. Quantum Technol. **7**, 6 (2020).
[22] A. Sesana *et al.*, Exp. Astron. **51**, 1333 (2021).
[23] J. Garcia-Bellido, H. Murayama, and G. White, J. Cosmol. Astropart. Phys. 12 (2021) 023.
[24] C. L. Carilli and S. Rawlings, New Astron. Rev. **48**, 979 (2004).
[25] G. Janssen *et al.*, *Proc. Sci.*, AASKA14 (2015) 037 [arXiv:1501.00127].
[26] A. Weltman *et al.*, Pub. Astron. Soc. Aust. **37**, e002 (2020).
[27] L. Lentati *et al.* (EPTA Collaboration), Mon. Not. R. Astron. Soc. **453**, 2576 (2015).
[28] S. Babak *et al.* (EPTA Collaboration), Mon. Not. R. Astron. Soc. **455**, 1665 (2016).
[29] Z. Arzoumanian *et al.* (NANOGRAV Collaboration), Astrophys. J. **859**, 47 (2018).
[30] K. Aggarwal *et al.*, Astrophys. J. **880**, 2 (2019).
[31] Z. Arzoumanian *et al.* (NANOGrav Collaboration), Astrophys. J. Lett. **905**, L34 (2020).
[32] G. Agazie *et al.* (NANOGrav Collaboration), Astrophys. J. Lett. **951**, L8 (2023).
[33] A. Afzal *et al.* (NANOGrav Collaboration), Astrophys. J. Lett. **951**, L11 (2023); **971**, L27(E) (2024).
[34] C. Caprini, M. Hindmarsh, S. Huber, T. Konstandin, J. Kozaczuk, G. Nardini, J. M. No, A. Petiteau, P. Schwaller, G. Servant, and D. J. Weir, J. Cosmol. Astropart. Phys. 04 (2016) 001.
[35] R. R. Caldwell, T. L. Smith, and D. G. E. Walker, Phys. Rev. D **100**, 043513 (2019).
[36] L. A. Boyle and P. J. Steinhardt, Phys. Rev. D **77**, 063504 (2008).
[37] L. A. Boyle and P. J. Steinhardt, Phys. Rev. D **77**, 063504 (2008).
[38] B. Barman, A. Ghoshal, B. Grzadkowski, and A. Socha, J. High Energy Phys. 07 (2023) 231.
[39] M. Hindmarsh, S. J. Huber, K. Rummukainen, and D. J. Weir, Phys. Rev. D **92**, 123009 (2015).
[40] A. Vilenkin, Phys. Rev. D **23**, 852 (1981).
[41] T. Vachaspati and A. Vilenkin, Phys. Rev. D **31**, 3052 (1985).
[42] J. J. Blanco-Pillado and K. D. Olum, Phys. Rev. D **96**, 104046 (2017).
[43] T. Hiramatsu, M. Kawasaki, and K. Saikawa, J. Cosmol. Astropart. Phys. 05 (2010) 032.
[44] R. Roshan, arXiv:2604.25726.
[45] R. A. Battye, L. P. Bunio, S. J. Cotterill, and P. B. G. Manoj, Phys. Rev. D **113**, 123540 (2026).
[46] M. Pearce, L. Pearce, G. White, and C. Balázs, J. Cosmol. Astropart. Phys. 06 (2024) 021.
[47] G. Barenboim and W.-I. Park, Phys. Lett. B **759**, 430 (2016).
[48] H. Assadullahi and D. Wands, Phys. Rev. D **79**, 083511 (2009).
[49] L. Alabidi, K. Kohri, M. Sasaki, and Y. Sendouda, J. Cosmol. Astropart. Phys. 05 (2013) 033.
[50] K. Kohri and T. Terada, Phys. Rev. D **97**, 123532 (2018).
[51] K. Inomata, K. Kohri, T. Nakama, and T. Terada, Phys. Rev. D **100**, 043532 (2019).
[52] O. Ferreira, E. S. Fraga, M. Hippert, and J. Schaffner-Bielich, Phys. Rev. D **112**, 094009 (2025).
[53] O. Ferreira, E. S. Fraga, and J. Schaffner-Bielich, arXiv:2603.26946.
[54] A. Spalding and S. F. King, arXiv:2605.28804.
[55] N. Seto and J. Yokoyama, J. Phys. Soc. Jpn. **72**, 3082 (2003).
[56] L. A. Boyle and A. Buonanno, Phys. Rev. D **78**, 043531 (2008).
[57] S. Kuroyanagi, T. Chiba, and N. Sugiyama, Phys. Rev. D **79**, 103501 (2009).
[58] K. Nakayama and J. Yokoyama, J. Cosmol. Astropart. Phys. 01 (2010) 010.
[59] S. Kuroyanagi, C. Ringeval, and T. Takahashi, Phys. Rev. D **87**, 083502 (2013).
[60] R. Jinno, T. Moroi, and K. Nakayama, J. Cosmol. Astropart. Phys. 01 (2014) 040.

[61] K. Saikawa and S. Shirai, J. Cosmol. Astropart. Phys. 05 (2018) 035.
[62] C. Chen, K. Dimopoulos, C. Eröncel, and A. Ghoshal, Phys. Rev. D **110**, 063554 (2024).
[63] W. Iania and A. Ricciardone, arXiv:2604.13012.
[64] D. J. H. Chung, E. W. Kolb, and A. Riotto, Phys. Rev. D **60**, 063504 (1999).
[65] S. Datta, A. Ghoshal, A. Spalding, and G. White, J. High Energy Phys. 03 (2026) 245.
[66] A. Ghoshal, A. Spalding, and G. White, Phys. Rev. D **114**, 035001 (2026).
[67] J. McDonald, Phys. Rev. D **43**, 1063 (1991).
[68] T. Moroi and L. Randall, Nucl. Phys. **B570**, 455 (2000).
[69] L. Visinelli and P. Gondolo, Phys. Rev. D **81**, 063508 (2010).
[70] A. L. Erickcek, Phys. Rev. D **92**, 103505 (2015).
[71] A. E. Nelson and H. Xiao, Phys. Rev. D **98**, 063516 (2018).
[72] A. Cheek, J. K. Osiński, and L. Roszkowski, J. Cosmol. Astropart. Phys. 03 (2024) 061.
[73] M. Cirelli, Y. Gouttenoire, K. Petraki, and F. Sala, J. Cosmol. Astropart. Phys. 02 (2019) 014.
[74] Y. Gouttenoire, G. Servant, and P. Simakachorn, J. Cosmol. Astropart. Phys. 07 (2020) 016.
[75] R. Allahverdi *et al.*, Open J. Astrophys. **4**, 1 (2021).
[76] R. Allahverdi and J. K. Osiński, Phys. Rev. D **105**, 023502 (2022).
[77] R. Allahverdi, N. P. D. Loc, and J. K. Osiński, Phys. Rev. D **107**, 123510 (2023).
[78] H. Murayama, B. Noether, and J. Schütte-Engel, J. Cosmol. Astropart. Phys. 12 (2025) 027.
[79] Z. A. Borboruah, F. F. Deppisch, A. Ghoshal, and L. Malhotra, Phys. Rev. D **112**, 056003 (2025).
[80] A. Cheek, A. Ghoshal, and D. Paul, Phys. Rev. D **113**, 023509 (2026).
[81] A. Ghoshal, E. Megias, G. Nardini, and M. Quiros, J. High Energy Phys. 07 (2025) 277.
[82] R. Gonzalez Suarez, Acta Phys. Pol. B **52**, 953 (2021).
[83] L. Jeanty and B. Shuve, arXiv:2511.17934.
[84] L. Lee, C. Ohm, A. Soffer, and T.-T. Yu, Prog. Part. Nucl. Phys. **106**, 210 (2019).
[85] J. Alimena *et al.*, J. Phys. G **47**, 090501 (2020).
[86] C. B. Verhaaren *et al.*, Front. Phys. **10**, 967881 (2022).
[87] N. Okada, P. Sanyal, and R. K. Verma, arXiv:2604.00866.
[88] R. Acciarri *et al.* (DUNE Collaboration), arXiv:1512.06148.
[89] J. M. Berryman, A. de Gouvea, P. J. Fox, B. J. Kayser, K. J. Kelly, and J. L. Raaf, J. High Energy Phys. 02 (2020) 174.
[90] B. Batell, J. A. Evans, S. Gori, and M. Rai, J. High Energy Phys. 05 (2021) 049.
[91] D. Curtin *et al.*, Rep. Prog. Phys. **82**, 116201 (2019).
[92] G. Bernardi *et al.*, Phys. Lett. **166B**, 479 (1986).
[93] D. Gorbunov, I. Krasnov, and S. Suvorov, Phys. Lett. B **820**, 136524 (2021).
[94] M. Anelli *et al.* (SHiP Collaboration), arXiv:1504.04956.
[95] M. Berbig and A. Ghoshal, J. High Energy Phys. 05 (2023) 172.
[96] Z. A. Borboruah, A. Ghoshal, L. Malhotra, and U. Yajnik, Phys. Rev. D **112**, 095017 (2025).
[97] Z. A. Borboruah, A. Ghoshal, and S. Ipek, J. High Energy Phys. 07 (2024) 228.
[98] N. Bernal, A. Ghoshal, F. Hajkarim, and G. Lambiase, J. Cosmol. Astropart. Phys. 11 (2020) 051.
[99] S. Datta and R. Samanta, J. High Energy Phys. 11 (2022) 159.
[100] S. Datta and R. Samanta, Phys. Rev. D **108**, L091706 (2023).
[101] M. Chianese, S. Datta, R. Samanta, and N. Saviano, J. Cosmol. Astropart. Phys. 11 (2024) 051.
[102] A. Ghoshal, L. Heurtier, and A. Paul, J. High Energy Phys. 12 (2022) 105.
[103] S. Datta, A. Ghosal, A. Ghoshal, and G. White, Phys. Rev. D **112**, 015009 (2025).
[104] K. Nakayama and Y. Tang, Phys. Lett. B **788**, 341 (2019); **839**, 137787(E) (2023).
[105] A. Ghoshal, R. Samanta, and G. White, Phys. Rev. D **108**, 035019 (2023).
[106] K.-Y. Choi, E. Lkhagvadorj, and S. Mahapatra, J. Cosmol. Astropart. Phys. 07 (2024) 064.
[107] A. Strumia and G. Landini, J. High Energy Phys. 04 (2025) 068.
[108] K. Nakayama, F. Takahashi, and J. Wada, Phys. Rev. D **113**, 056008 (2026).
[109] R. Allahverdi and M. Drees, Phys. Rev. Lett. **89**, 091302 (2002).
[110] T. Bringmann, P. F. Depta, M. Hufnagel, J. T. Ruderman, and K. Schmidt-Hoberg, Phys. Rev. Lett. **127**, 191802 (2021).
[111] J. Preskill, M. B. Wise, and F. Wilczek, Phys. Lett. **120B**, 127 (1983).
[112] L. F. Abbott and P. Sikivie, Phys. Lett. **120B**, 133 (1983).
[113] M. Dine and W. Fischler, Phys. Lett. **120B**, 137 (1983).
[114] M. S. Turner, Phys. Rev. D **28**, 1243 (1983).
[115] O. Lebedev, J. Cosmol. Astropart. Phys. 02 (2023) 032.
[116] D. Feiteira and O. Lebedev, J. Cosmol. Astropart. Phys. 07 (2025) 003.
[117] A. Mierna, G. Perna, S. Matarrese, N. Bartolo, and A. Ricciardone, arXiv:2507.08737.
[118] F. D'Eramo and K. Schmitz, Phys. Rev. Res. **1**, 013010 (2019).
[119] M. Chianese, S. Datta, G. Miele, R. Samanta, and N. Saviano, Phys. Rev. D **111**, L041305 (2025).
[120] A. Ghoshal, D. Paul, and S. Pal, J. High Energy Phys. 12 (2024) 150.
[121] Y. Akrami *et al.* (Planck Collaboration), Astron. Astrophys. **641**, A10 (2020).
[122] D. Langlois, Lect. Notes Phys. **800**, 1 (2010).
[123] K. Kadota, M. Kawasaki, and K. Saikawa, J. Cosmol. Astropart. Phys. 10 (2015) 041.
[124] T. Hiramatsu, M. Kawasaki, and K. Saikawa, J. Cosmol. Astropart. Phys. 02 (2014) 031.
[125] C. Tian, X. Wang, and C. Balázs, J. Cosmol. Astropart. Phys. 08 (2025) 060.
[126] J. Ellis, M. Lewicki, and V. Vaskonen, J. Cosmol. Astropart. Phys. 11 (2020) 020.
[127] J. L. Feng, I. Galon, F. Kling, and S. Trojanowski, Phys. Rev. D **97**, 055034 (2018).